Journal of Catalysis **204,** 89–97 (2001)
doi:10.1006/jcat.2001.3382, available online at http://www.idealibrary.com on IDEAL®

Role of Potassium in Carbon-Free CO_2 Reforming of Methane on K-Promoted Ni/Al_2O_3 Catalysts

Toshihiko Osaki[1] and Toshiaki Mori[2]

National Institute of Advanced Industrial Science and Technology (AIST), 2266-98, Anagahora, Shimoshidami, Moriyama-ku, Nagoya 463-8560, Japan

Received March 5, 2001; revised August 3, 2001; accepted August 3, 2001

In order to reveal the role of alkali in the carbon-free CO_2 reforming of methane, the kinetics of the individual steps involved in the reforming were examined on Ni/Al_2O_3 catalysts with 0, 1, 5, and 10 wt% K. Although the adsorption of CO_2 was enhanced by the presence of potassium, the dissociation of CO_2 to CO and O_{ads} was not significantly influenced. This suggests that the enhancement of the oxidation of $CH_{X,ads}$ by increasing the concentration of O_{ads} is not the cause for the carbon-free CO_2 reforming. The carbon-free reforming was mainly ascribed to the ensemble control; i.e., potassium plays a role in dividing the nickel surface into the smaller ensembles and, thereby, the carbon deposition is suppressed. On the other hand, the rate-determining step, ascribed to the dissociation of CH_XO_{ads} to CO and $x/2H_2$, was not affected by potassium below the threshold coverage of $\Theta_K =$ ca. 0.4, but above it, the rate became slow. The number of surface nickel atoms (nickel ensemble) required for the reforming was estimated from a simple Langmuir form, $r = r_0(1 - \Theta_K)^n$, to be ca. 2.9. The number was similar to that obtained on sulfur-passivated Ni catalysts in H_2O reforming of methane, suggesting that the retardation of the rate-determining step at $\Theta_K > 0.4$ is ascribed to the physical blockage of the nickel ensemble by potassium.

Key Words: **carbon-free CO_2 reforming; CH_4; nickel; potassium; ensemble; CO_2 dissociation; rate-determining step; reverse-Boudouard reaction.**

INTRODUCTION

In H_2O or CO_2 reforming of hydrocarbons, supported Ni catalysts are active and commonly used in industries due to the low cost (1–3). However, nickel catalysts can easily induce carbon deposition, which is caused by methane decomposition and the disproportionation of carbon monoxide, resulting in catalyst deactivation and plugging of a reactor tube. To prevent carbon formation, the addition of alkali or alkaline-earth metal oxides to nickel is a well-known technique (4–8). The addition resulted in the increased negative values of reaction order with respect to the partial pressure of H_2O (7) and CO_2 (8), although the reaction orders for the CO_2 reforming of methane are controversial (8–11). On the other hand, it should also be noted that the basic metal oxides reduced not only the coking rate but also the reforming rate (7, 8): in some cases, the reforming rate decreased by more than one order of magnitude.

The role of alkali or alkaline-earth metal oxides has been discussed in terms of either the geometric or the electronic nature of the catalyst surface influencing the activity and the selectivity of reactions. The importance of the geometric factor was proposed by Balandin and Kobozev in the multiplet (12) and ensemble (13) theories, respectively. On the other hand, Dowden stressed the importance of the electronic factor with the advent of the band theory of the electronic states of solids (14). Quantum mechanical calculations for Ni(111) showed that adsorbed potassium atoms have a significant impact on the electronic properties of surface nickel atoms (15). Electrostatic calculations using medium theory showed that alkali promotes the adsorption of steam on nickel (16). A recent surface science study revealed that the methane sticking probability is strongly diminished by the presence of potassium atoms (17). However, it was also reported that the addition of alkali to the nickel surface does not change the methane adsorption rate and the activation energy due to its nonpolar structure (18). It was speculated that alkali enhances the reconstruction (faceting) of an active nickel surface to a less active one resulting in the reduction of both coking and reforming activities (19–22), although further studies seem necessary to verify the facetting mechanism.

More fundamental studies are still needed to reveal the role of alkali in the carbon-free reforming of methane. In the CO_2 reforming of methane, many individual steps are involved, as depicted in Fig. 1 (23–27): CH_4 dissociation to $CH_{X,ads}$ and $(4-x)/2H_2$ (k_1), further dissociation of $CH_{X,ads}$ to C and $x/2H_2$ (k_2), CO_2 dissociation to CO and O_{ads} (k_3), the surface reaction between $CH_{X,ads}$ and O_{ads} to give CH_XO_{ads} (k_4), a subsequent rate-determining step $CH_XO_{ads} \rightarrow CO + x/2H_2$ (k_5) (27, 28), and the gasification

[1] To whom correspondence should be addressed. Fax: 81-52-736-7400. E-mail: t-osaki@aist.go.jp.

[2] Present address: Department of Materials Science and Technology, Faculty of Science and Technology, Hirosaki University, Bunkyo-cho, Hirosaki 036-8561, Japan.

0021-9517/01 $35.00

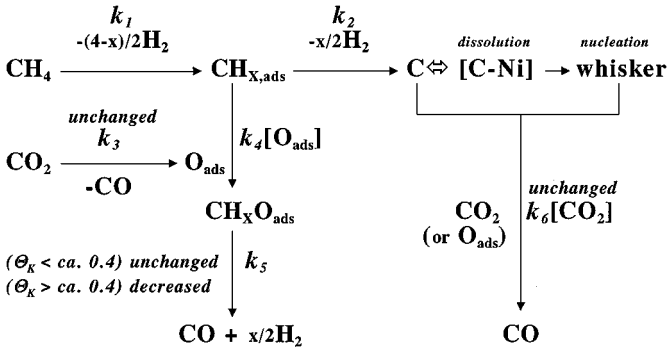

FIG. 1. Influence of potassium on the rates of individual steps involved in the CH_4–CO_2 reaction.

of deposited carbon by CO_2 (k_6). In this study, to reveal the role of alkali in reforming, the rates of individual steps involved in methane reforming were investigated using 0, 1, 5, and 10 wt% K-promoted Ni/Al_2O_3 catalysts.

EXPERIMENTAL

K-Ni/Al_2O_3 catalysts (Ni = 20 wt%, K = 0, 1, 5, and 10 wt%) were prepared as follows: γ-Al_2O_3 (GL Science; particle size: 0.30–0.59 mm, surface area: 111.6 $m^2\ g^{-1}$) was impregnated in an aqueous solution of nickel nitrate followed by drying and subsequently calcining at 773 K for 3 h. An appropriate amount of potassium was then added by impregnation using an aqueous solution of potassium carbonate, followed by drying and further calcining at 773 K for 3 h. Before catalytic reactions, the catalyst was reduced with hydrogen (30 ml min^{-1}) at 773 K for 3 h followed by passing helium (30 ml min^{-1}) at 773 K for 10 min.

Temperature-programmed reduction (TPR) was performed in a 5% H_2–Ar carrier gas (60,000 ml h^{-1} g-cat.$^{-1}$) at a constant ramping rate of 5 K min^{-1} from room temperature to 1273 K. The amount of CO adsorbed on the catalyst was measured by a conventional pulse adsorption apparatus at room temperature after catalyst reduction. X-ray powder diffraction analysis was carried out to estimate the Ni crystallite size using a Rigaku RAD-1VC with filtered Cu$K\alpha$ (30 kV, 20 mA) radiation.

Steady-state CO_2 reforming was carried out under differential reactor conditions. The flow rate was 360,000 ml h^{-1} g-cat.$^{-1}$ ($CH_4:CO_2 = 1:1$) at atmospheric pressure without using a diluent. The effluent gas from the reactor (4-mm-i.d. quartz glass tube) was analyzed by on-line gas chromatography with a thermal conductivity detector. Turnover frequency (TOF) was calculated from the CH_4 conversion rate using the amount of CO adsorbed.

Carbon formation on the catalyst was investigated by thermogravimetry (TG, Shimadzu TGA-50) using a TG quartz basket, on which the catalyst was placed. After catalyst reduction followed by flowing helium, CH_4 (40 ml min^{-1}) or CH_4–CO_2 (1 : 1, 40 ml min^{-1}) was flowed over the catalyst, and the weight increase due to carbon accumulation was monitored continuously.

The ability of the catalyst to dissociate CO_2 was investigated by a pulse reaction technique. After catalyst reduction followed by purging hydrogen with helium, CO_2 (0.80 ml) was pulsed onto the catalyst in helium carrier gas (9000 ml h^{-1} g-cat.$^{-1}$) at 773 K several times. The effluent gas (CO_2 and CO) was analyzed by on-line gas chromatography with a thermal conductivity detector using a separation column of active carbon. The conversion of CO_2 to CO and O_{ads} (%) was calculated from $100 \times (N_{CO}/N^0_{CO_2})$, where N_{CO} is the amount of CO detected by gas chromatography and $N^0_{CO_2}$ is the amount of CO_2 pulsed. The amount of CO_2 adsorbed on the catalyst in the pulse reaction was estimated from the carbon balance between the amount of CO_2 pulsed and those of CO and CO_2 detected by gas chromatography; i.e., adsorbed $CO_2(\%) = 100 \times \{N^0_{CO_2} - (N_{CO_2} + N_{CO})\}/N^0_{CO_2}$, where N_{CO_2} is the amount CO_2 detected by gas chromatography.

Pulse surface reaction rate analysis (PSRA) was carried out in a CO_2–He carrier gas (3 : 37, 12,000 ml h^{-1} g-cat.$^{-1}$) as performed in previous studies (23–26). The apparatus was composed of a pulse microreactor (4-mm-i.d. quartz glass tube) connected directly to a quadrupole mass spectrometer (Anelva AGS-120). Via the carrier gas, CH_4 (ca. 0.24 ml) was pulsed onto the catalyst (ca. 200 mg), and a small part of the effluent gas from the reactor was introduced to the mass spectrometer through a variable leak valve. The dynamic behavior of CO (m/z 28) and H_2 (m/z 2) was monitored continuously.

The effect of potassium on the gasification of carbon by CO_2 was investigated by TG. After catalyst reduction in a TG quartz cell followed by passing helium, CH_4 (40 ml min^{-1}) was flowed over the catalyst for carbon formation at 773 K. After purging CH_4 with helium at 773 K for 10 min, CO_2 (40 ml min^{-1}) was flowed over the catalyst at 773 K and the weight decrease due to the reverse-Boudouard reaction ($C + CO_2 \rightarrow 2CO$) was monitored continuously.

The reactivity of deposited carbon was also investigated by temperature-programmed hydrogenation (TPH). After catalyst reduction followed by purging hydrogen with helium, CH_4 (36,000 ml h^{-1} g-cat.$^{-1}$) was flowed over the catalyst at 773 K for 1 min. After purging CH_4 with helium, the catalyst was cooled down to room temperature in helium carrier gas, and TPH was performed in hydrogen carrier gas (36,000 ml h^{-1} g-cat.$^{-1}$) from room temperature to 1273 K heating at a rate of 5 K min^{-1}.

RESULTS

TPR spectra of K-NiO/Al_2O_3 catalysts are shown in Fig. 2. The spectra of 0, 1, and 5 wt% K-NiO/Al_2O_3 exhibited mainly two reduction peaks around 400°C, while

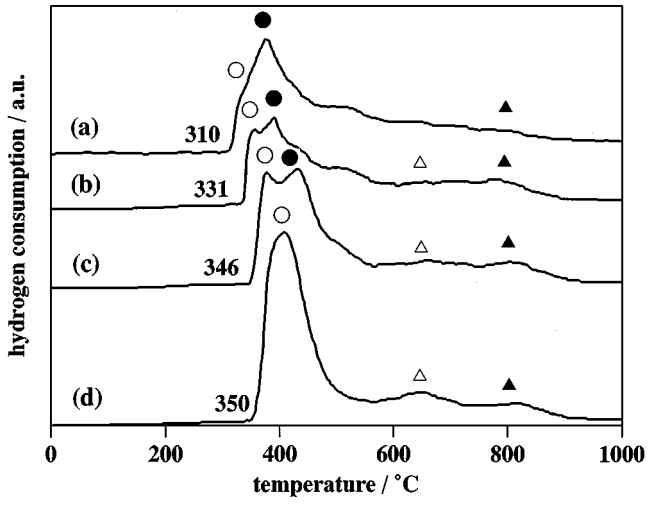

FIG. 2. TPR profiles of (a) NiO/Al_2O_3 (30.0 mg), (b) 1 wt% K-NiO/Al_2O_3 (30.1 mg), (c) 5 wt% K-NiO/Al_2O_3 (30.3 mg), and (d) 10 wt% K-NiO/Al_2O_3 (30.0 mg). The denoted number indicates the temperature at which the reduction starts.

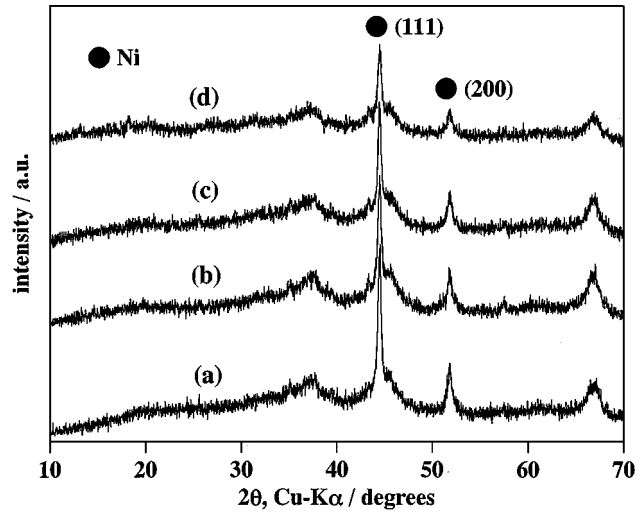

FIG. 3. XRD patterns of (a) Ni/Al_2O_3, (b) 1 wt% K-Ni/Al_2O_3, (c) 5 wt% K-Ni/Al_2O_3, and (d) 10 wt% K-Ni/Al_2O_3.

that of 10 wt% K-NiO/Al_2O_3 showed one. The reduction peak appearing at a lower temperature became larger with K concentration, while that at a higher temperature became smaller, and the latter reduction peak disappeared on 10 wt% K-NiO/Al_2O_3. Both reduction peaks shifted to a higher temperature with increasing K concentration. The temperature at which the reduction started also shifted to a higher temperature as K wt% increased. In the spectra, two additional peak maxima were observed at ca. 650 and 800°C. The former might be ascribed to the reduction of nickel oxide strongly interacting with potassium, because the peak became larger with K wt%, while the latter may be due to the reduction of nickel aluminate ($NiAl_2O_4$) formed by the reaction between nickel and aluminum oxide during the calcination step (29).

Figure 3 shows X-ray diffraction (XRD) spectra of catalysts after reduction at 773 K. The spectra exhibited two Ni diffraction lines corresponding to the (111) and (200) planes. The Ni crystallite size was calculated from the line broadening using the Scherrer equation and the results are shown in Table 1. The Ni crystallite size was ca. 20–23 nm which suggests that the addition of potassium hardly influences the particle size of nickel. Since Warren's correction for instrumental line broadening was not used in the Scherrer equation, the values obtained are slightly lower than the true ones. In Table 1, the amount of CO adsorbed on the catalysts is also shown. The amount decreased with an increase in K wt%, indicating that potassium covered the surface of nickel. The surface-weighted particle size of the unpromoted Ni/Al_2O_3 catalyst was roughly estimated from the CO chemisorption via 100/(Ni dispersion (%)) to be ca. 25.9 nm, indicating good agreement with the values obtained from XRD. The coverage of Ni by K (Θ_K), which was calculated from the decrease of CO adsorption, increased with increasing K concentration. The active Ni surface area per gram catalyst, as estimated using CO adsorption and Ni atom area (6.5×10^{-20} m^2 $atom^{-1}$), was 2.9–5.1 m^2 $g\text{-}cat.^{-1}$.

Figure 4 shows the results of steady-state CH_4–CO_2 reaction under differential reactor conditions (CH_4 conversion below 7%). The TOF was almost the same when potassium concentration was below 5 wt%, while it decreased when 10 wt% potassium was added. The results are qualitatively in accordance with those reported in a previous study (8), i.e., with the exception of Na_2O, the addition of alkali or alkaline–earth metal oxides to nickel resulted in the reduction of TOF. The apparent activation energies were calculated to be 62 and 115 kJ mol^{-1} for 0–5 and 10 wt% K-Ni/Al_2O_3 catalysts, respectively, which are comparable to those reported on Ni/MgO (92 kJ mol^{-1}), Ni/SiO_2 (96 kJ mol^{-1}), and Ni/C (121 kJ mol^{-1}) (28). The TOF obtained is also comparable to that on Ni/C (1.4 s^{-1}), Ni/SiO_2 (0.9 s^{-1}), and Ni/MgO (0.1 s^{-1}) at 773 K (28).

TABLE 1

Characterization of K-Ni/Al_2O_3 Catalysts

Catalyst	Ni crystallite size (nm)	CO adsorption (μmol g^{-1})	Ni coverage (Θ_K)	Ni surface area (m^2 g^{-1})
Ni/Al_2O_3	22.9[a] (21.7)[b]	131.1	(0)	5.1
1 wt% K-Ni/Al_2O_3	21.8 (20.2)	103.0	0.21	4.0
5 wt% K-Ni/Al_2O_3	22.9 (20.2)	88.0	0.33	3.4
10 wt% K-Ni/Al_2O_3	19.6 (23.5)	73.5	0.44	2.9

[a] Ni (111).
[b] Ni (200).

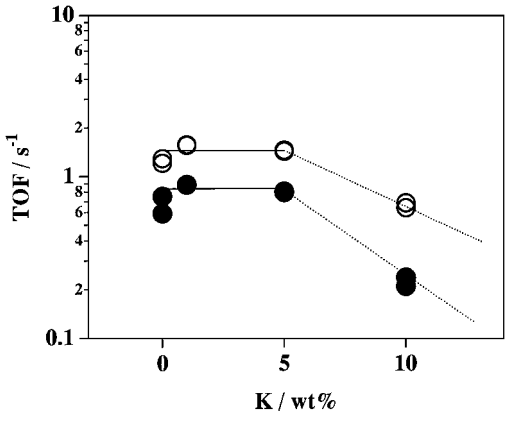

FIG. 4. TOF for steady-state CH_4–CO_2 reaction at 773 K (●) and 823 K (○). Catalyst weight: Ni/Al_2O_3 (10.0 mg), 1 wt% K-Ni/Al_2O_3 (10.0 mg), 5 wt% K-Ni/Al_2O_3 (10.0 mg), and 10 wt% K-Ni/Al_2O_3 (10.2 mg).

Carbon formation during catalyst exposure to CH_4 at 773 K is shown in Fig. 5, where the results show that carbon formation was suppressed with increasing K loading. Similar results were obtained during catalyst exposure to CH_4–CO_2, as shown in Fig. 6. On each K-Ni/Al_2O_3 catalyst, carbon formation was suppressed more markedly in the presence of CO_2 than in the absence of CO_2. Especially on 5 and 10 wt% K-Ni/Al_2O_3, very little carbon formation was observed during the CH_4–CO_2 reaction, although the ability for carbon formation still remained in the absence of CO_2. The apparent rate of carbon formation was estimated from the initial slope of the carbon formation profile, and Fig. 7 shows the rate per site of catalyst (r_{coke}/s^{-1}) in the presence and absence of CO_2. The r_{coke}/s^{-1} was calculated by $r_{coke} = (dW_C/dt)_0(1/M_C)(1/W_{cat})(1/S)$, where $(dW_C/dt)_0$/g s^{-1} is the initial carbon formation rate, M_C/g mol^{-1} is the atomic weight of carbon, W_{cat}/g is the weight of the catalyst, and S/mol g^{-1} is the CO adsorption number. Results indicate that (i) the carbon accumulation rate is slower in the presence of CH_4–CO_2 than in CH_4, and

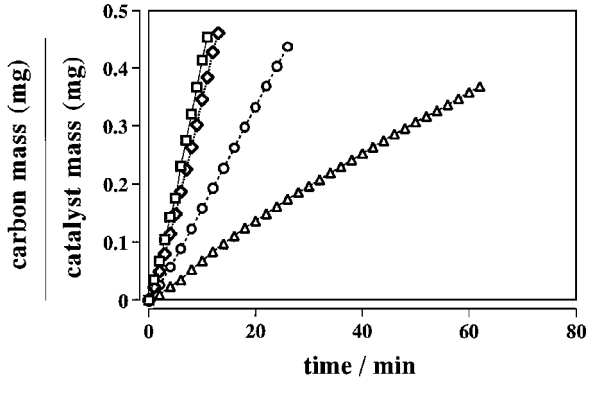

FIG. 5. TG in CH_4 at 773 K on Ni/Al_2O_3 (20.0 mg) □, 1 wt% K-Ni/Al_2O_3 (20.0 mg) ◇, 5 wt% K-Ni/Al_2O_3 (20.0 mg) ○, and 10 wt% K-Ni/Al_2O_3 (20.9 mg) △.

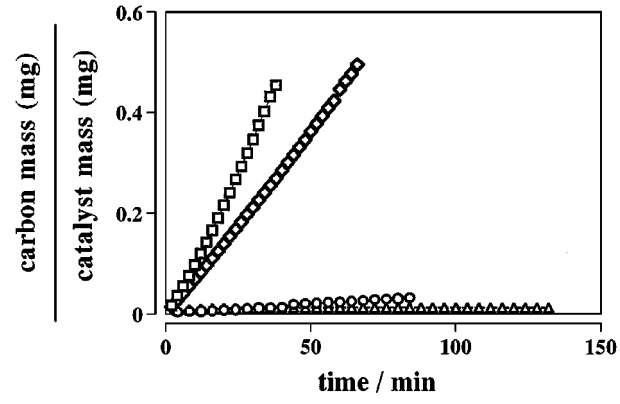

FIG. 6. TG in CH_4–CO_2 at 773 K on Ni/Al_2O_3 (20.0 mg) □, 1 wt% K-Ni/Al_2O_3 (20.0 mg) ◇, 5 wt% K-Ni/Al_2O_3 (20.0 mg) ○, and 10 wt% K-Ni/Al_2O_3 (20.9 mg) △.

(ii) the carbon accumulation rate decreases with potassium concentration in both atmospheres.

Figure 8 shows the results of sequential CO_2 pulses to the catalyst via helium carrier gas at 773 K. When CO_2 was pulsed onto the K-Ni/Al_2O_3 catalysts, a part of the CO_2 was adsorbed on the catalyst (Fig. 8a); the amount increased with an increase in potassium loading, indicating the enhancement of adsorption of CO_2 on K-promoted catalysts. On the 10 wt% K-Ni/Al_2O_3 catalyst, ca. 60% of the pulsed CO_2 was adsorbed in the first pulse. Figure 8b shows the conversion of CO_2 to CO and O_{ads}, which indicates that a part of the CO_2 pulsed was dissociatively adsorbed on the nickel surface to produce CO and O_{ads}. The CO_2 conversion decreased with K wt%, which is in contrast to the result for CO_2 adsorption. As for the first pulse onto the 10 wt% K-Ni/Al_2O_3 sample, a large part of CO_2 was adsorbed on the catalyst and, therefore, lower CO_2 conversion may be obtained. The apparent CO_2 dissociation rate

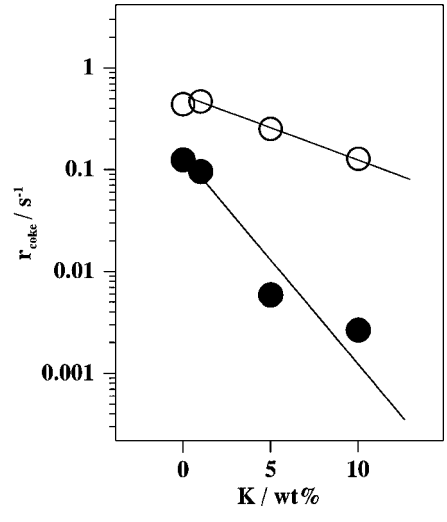

FIG. 7. The carbon formation rate per site of catalyst at 773 K in CH_4 (○) and CH_4−CO_2 (●).

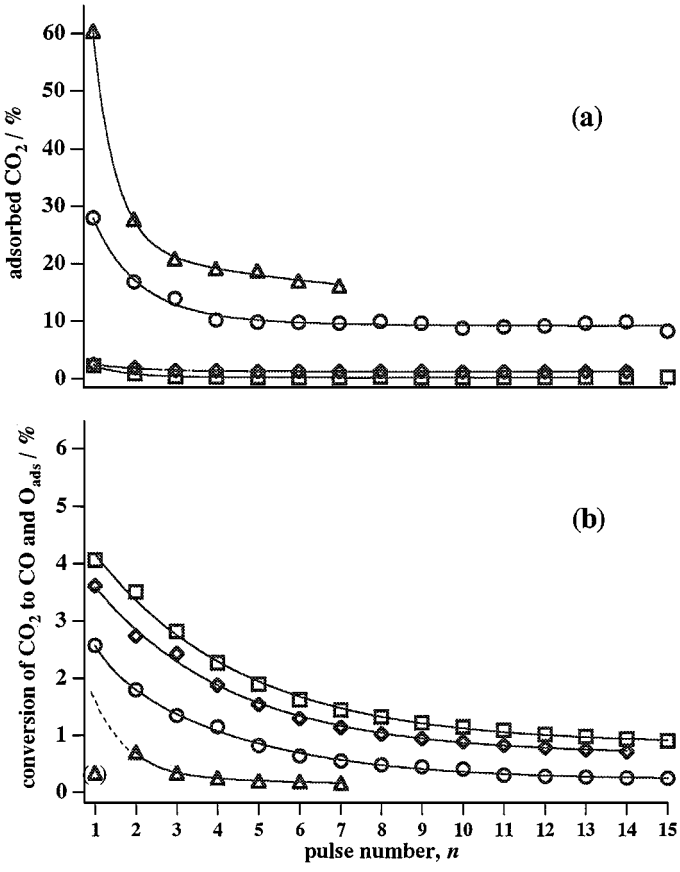

FIG. 8. (a) Adsorption of CO_2 and (b) conversion of CO_2 to CO and O_{ads} at 773 K in He on Ni/Al_2O_3 (200.2 mg) □, 1 wt% $K\text{-}Ni/Al_2O_3$ (199.8 mg) ◇, 5 wt% $K\text{-}Ni/Al_2O_3$ (199.4 mg) ○, and 10 wt% $K\text{-}Ni/Al_2O_3$ (200.2 mg) △.

per site of catalyst (N_{CO_2}/s^{-1}) was calculated using the CO_2 conversion for pulse number = 1, as summarized in Table 2. The rates were essentially the same among the catalysts except for 10 wt% $K\text{-}Ni/Al_2O_3$, for which significant adsorption of CO_2 was observed in the pulse reaction and, thereby, a precise value could not be obtained.

TABLE 2

Rates for the Dissociation of CO_2 to CO and O_{ads}

Catalyst	$N_{CO_2}{}^a$ (10^{-2} s^{-1})
Ni/Al_2O_3	3.5
1 wt% $K\text{-}Ni/Al_2O_3$	3.9
5 wt% $K\text{-}Ni/Al_2O_3$	3.3
10 wt% $K\text{-}Ni/Al_2O_3$	0.52[b]

[a] Apparent CO_2 dissociation rate $N_{CO_2}/s^{-1} = (F/W)(C/100)(1/S)$, where F/mol s^{-1} = carrier flow rate, W/g = catalyst weight, $C(\%)$ = conversion of CO_2 to $CO + O_{ads}$ at pulse number = 1, and S/mol g^{-1} = CO chemisorption number per catalyst weight.

[b] The value may not be valid because of the significant adsorption of CO_2 on the catalyst in the pulse reaction.

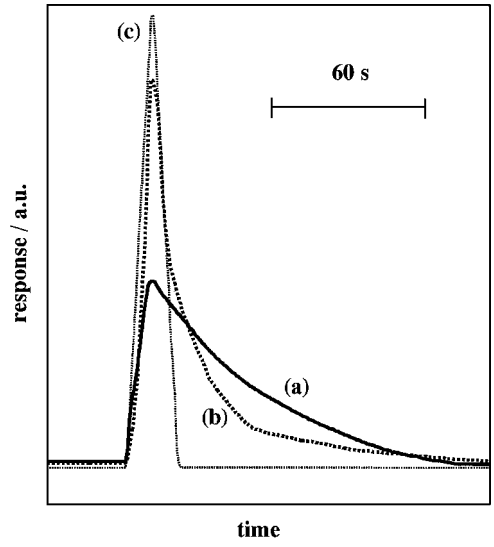

FIG. 9. (a) Tailing curves of CO and (b) H_2 produced from the CH_4–CO_2 reaction on 5 wt% $K\text{-}Ni/Al_2O_3$ catalyst at 733 K. (c) The sharp dotted line is for the response of the CO pulse.

Figure 9 shows the results of PSRA on a $K\text{-}Ni/Al_2O_3$ catalyst. The response for CO, h_{CO}, exhibited pronounced tailing after the CH_4 pulse. The response for H_2, h_{H_2}, showed a sharp peak in the initial period of reaction and tailing in the later period of reaction. The observed tailing curve was analyzed by assuming that the pulsed methane was irreversibly adsorbed on the catalyst to form an intermediate, X_{ads}, followed by the gradual conversion to products (23–26). If the rate of CO production r is proportional to the concentration of adsorbed species X_{ads}, then

$$r = -d[X_{ads}]/dt = k_X[X_{ads}], \qquad [1]$$

where k_X is the first-order rate constant, corresponding to k_5 in Fig. 1 (27). Since the height of tailing curve h at time t is proportional to the reaction rate r, the following equation can be solved by integrating Eq. [1];

$$\ln h = -k_X t + \text{constant}. \qquad [2]$$

The first-order rate constant k_X was calculated from the slope of the straight line for $\ln h_{CO}$ vs t plots. Figure 10 shows the Arrhenius plots for the rate constants at 713–743 K. The surface reaction rate constants were essentially the same among the catalysts except for 10 wt% $K\text{-}Ni/Al_2O_3$, for which smaller rate constants were obtained. The apparent activation energies were 64 and 111 kJ mol^{-1} for 0–5 and 10 wt% $K\text{-}Ni/Al_2O_3$ catalysts, respectively, which are in good agreement with those obtained for steady-state reaction. On the other hand, peak broadening of h_{H_2} in the initial period of reaction was not observed for K-added Ni/Al_2O_3 catalysts, although alkali is considered to increase the barrier for CH_4 dissociation (17).

To investigate the effect of potassium on the gasification of deposited carbon by CO_2, the kinetics of the

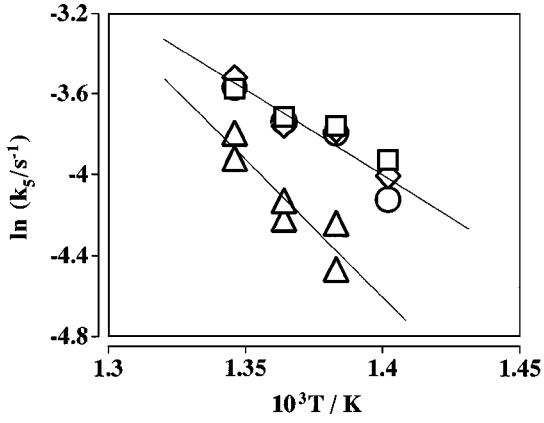

FIG. 10. Arrhenius plots of the rate constants for the CH_4–CO_2 reaction determined by PSRA on Ni/Al_2O_3 (□), 1 wt% K-Ni/Al_2O_3 (◇), 5 wt% K-Ni/Al_2O_3 (○), and 10 wt% K-Ni/Al_2O_3 (△).

reverse-Boudouard reaction were measured by TG. When methane was introduced to the catalyst in a TG quartz cell, an increase of the catalyst weight due to coking was observed. After a constant amount of carbon was formed, the replacement of carrier gas from CH_4 to CO_2 caused a gradual weight decrease due to the reverse-Boudouard reaction, $C + CO_2 \rightarrow 2CO$, as shown in Fig. 11. The rate of CO production was approximately expressed in terms of a first-order reaction with respect to the number of deposited carbon atoms, N_C, as analyzed in previous studies (24, 25). Figure 12 shows the relationship between $\ln(N_C/N_C^0)$ and time, where N_C^0 is N_C at $t = 0$, from the slope of which $k_6[CO_2]$ in Fig. 1 can be estimated. Straight lines were observed for all the catalysts, although slight deviation was observed in the later period of reaction. The slopes of the straight lines were essentially the same, strongly suggesting that potassium hardly affects the gasification of deposited carbon by CO_2.

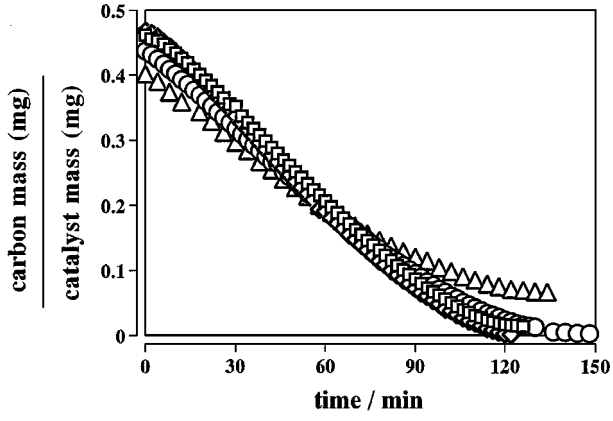

FIG. 11. Dynamics of the reverse-Boudouard reaction in CO_2 at 773 K on Ni/Al_2O_3 (20.0 mg) □, 1 wt% K-Ni/Al_2O_3 (20.0 mg) ◇, 5 wt% K-Ni/Al_2O_3 (20.0 mg) ○, and 10 wt% K-Ni/Al_2O_3 (20.9 mg) △.

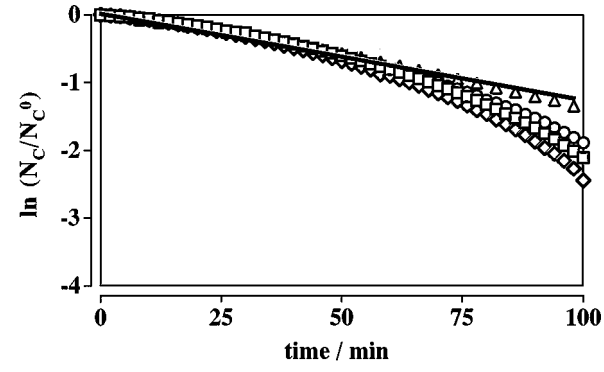

FIG. 12. Relationship between $\ln(N_C/N_C^0)$ and time on Ni/Al_2O_3 (□), 1 wt% K-Ni/Al_2O_3 (◇), 5 wt% K-Ni/Al_2O_3 (○), and 10 wt% K-Ni/Al_2O_3 (△).

The reactivity of deposited carbon was also investigated by TPH as shown in Fig. 13. The following aspects were observed from the profiles: (a) the amount of carbon deposited by CH_4 decomposition decreased with increasing potassium concentration, (b) one methanation peak was observed in the temperature range of 545–585°C, (c) the peak shifted to a lower temperature with increasing K loading except for 1 wt% K-Ni/Al_2O_3, and (d) the temperature at which methanation started was almost the same for all the catalysts, namely, 460°C. The observed peak shift to a lower temperature may be due to the difference in the amount of carbon deposited; e.g., the amount of carbon formed on 10 wt% K-Ni/Al_2O_3 was about 1/5 that on Ni/Al_2O_3, which may result in the shift of the peak to a

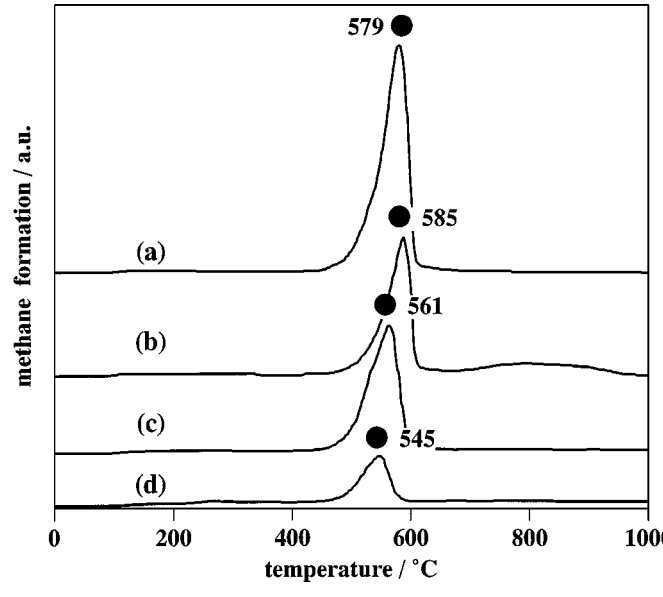

FIG. 13. TPH profiles in H_2 for (a) Ni/Al_2O_3 (25.0 mg) + Al_2O_3 (25.2 mg), (b) 1 wt% K-Ni/Al_2O_3 (25.2 mg) + Al_2O_3 (26.0 mg), (c) 5 wt% K-Ni/Al_2O_3 (25.0 mg) + Al_2O_3 (25.0 mg), and (d) 10 wt% K-Ni/Al_2O_3 (25.3 mg) + Al_2O_3 (25.5 mg).

lower temperature despite the same temperature (460°C) at which the methanation started. The difference in the reactivity of deposited carbon is, therefore, almost negligible on K-promoted Ni catalysts as indicated by the analysis of the reverse-Boudouard reaction.

DISCUSSION

Irreversible CO adsorption on K-Ni/Al_2O_3 catalysts decreases with increasing potassium concentration, as shown in Table 1. TPR also showed a shift to higher temperature in NiO reduction with potassium content, as depicted in Fig. 2. On the other hand, the nickel particle size was not significantly influenced by potassium, as revealed by XRD line broadening (Table 1). These results strongly suggest that a portion of nickel particles was covered with potassium. It is considered that a less acidic support like alumina has a weaker bonding of alkali, resulting in easier adsorption of potassium onto the nickel metal surface (21, 22).

Carbon formation on the catalysts during exposure to either CH_4 (Fig. 5) or a CH_4–CO_2 mixture (Fig. 6) was suppressed by the addition of potassium, while the reforming activity was suppressed at 10 wt% K (Fig. 4). These results indicate that potassium can reduce not only the coking activity but also the reforming activity. To investigate the role of potassium in carbon-free CO_2 reforming, the kinetics of individual steps involved in the CH_4–CO_2 reaction were examined. As shown in Fig. 9, CH_4 was dissociatively adsorbed on Ni to produce $CH_{X,\mathrm{ads}}$ and $(4-x)/2H_2$ in the initial period of reaction; however, broadening of the initial sharp peak was not observed even at high K concentrations. Although it seems that potassium does not affect the CH_4 dissociation, further studies are necessary to reveal more precisely the kinetics of CH_4 dissociation. It is revealed that the sticking probability is strongly diminished by the presence of potassium (17). Density functional theory calculations show that the energy barrier for the dissociation of CH_4 is increased when potassium is present on a nickel surface due to the interaction between the induced dipole moment in the transition state and the electrostatic field induced by the potassium atoms. In PSRA, the degree of dehydrogenation of CH_X in CO_2 reforming is found to be small on Ni supported on MgO but large on Ni supported on SiO_2 despite the similar TOF for reforming (23, 24). A similar effect was recently reported for H_2O reforming of methane; i.e., the reforming rate per site of catalyst is almost the same between Ni catalysts supported on MgO and $MgAl_2O_4$, while H-D exchange in CD_4–H_2 (5:95) is lower on Ni supported on MgO compared to Ni on $MgAl_2O_4$ (22). These results indicate that basic metal oxides can influence the degree of dehydrogenation of $CH_{X,\mathrm{ads}}$ species.

The enhancement of CO_2 adsorption on K-promoted Ni/Al_2O_3 catalysts was found in the pulse reaction, as shown in Fig. 8a. CO_2 adsorption is observed on alkali or alkaline–earth metal oxide-promoted Al_2O_3, even at elevated temperatures above 773 K (30), suggesting that CO_2 adsorption on the K-Ni/Al_2O_3 catalysts is due to the strong interaction between acidic CO_2 and the basic catalyst surface modified by potassium. However, the rate of CO_2 dissociation to CO and O_{ads} was not significantly influenced by potassium, as shown in Table 2. These results indicate that potassium promotes the adsorption of CO_2 on the catalyst surface, but does not necessarily affect the rate of CO_2 dissociation. In a previous study (8), the reaction rate laws observed on an alumina-supported Ni catalyst (Eq. [3]) and on a catalyst promoted by CaO (Eq. [4]) were

$$r = kP_{\mathrm{CH_4}}^{-0.27}P_{\mathrm{CO_2}}^{0.21}, \quad [3]$$

$$r = kP_{\mathrm{CH_4}}^{0.38}P_{\mathrm{CO_2}}^{-0.57}, \quad [4]$$

in which the reaction order is negative with respect to CH_4 partial pressure and positive with respect to CO_2 partial pressure on Ni/Al_2O_3, while it is positive with respect to CH_4 partial pressure and negative with respect to CO_2 partial pressure on CaO-promoted Ni/Al_2O_3. For Ni/Al_2O_3 catalysts, it is also reported that the reaction order is in the range of 0.55–1.0 with respect to CH_4 partial pressure while it is 0–0.35 with respect to CO_2 partial pressure (9–11), which conflicts with Eq. [3]. This conflict might be due to the difference in the reaction conditions examined; e.g., the difference in the partial pressure range examined might largely contribute to it, because the dependence is complex over a wide range of both partial pressures (11, 31). For CaO-promoted Ni/Al_2O_3 catalysts (Eq. [4]), the negative reaction order with respect to CO_2 partial pressure may be explained as a result of the inhibition of the overall reaction due to the strong adsorption of CO_2 onto the active sites modified by CaO. Although further examination is still necessary to clarify the effect of alkali on the dissociative adsorption of CO_2, it is considered that carbon-free reforming is not ascribed to the enhancement of the oxidation of $CH_{X,\mathrm{ads}}$ by atomic oxygen (k_4), because concentration of O_{ads} formed by CO_2 dissociation (k_3) is not increased by alkali (Table 2).

The subsequent rate-determining step (27, 28), assumed to be $CH_XO_{\mathrm{ads}} \rightarrow CO + x/2H_2$ (k_5), was examined by PSRA, as shown in Fig. 10. The estimated rate constants were essentially the same among the catalysts except for 10 wt% K-Ni/Al_2O_3, for which k_5 was smaller. The activity pattern was the same as that during steady-state CO_2 reforming, as shown in Fig. 4, and the activation energies also agreed well with those for the steady-state reaction. To estimate the critical size of active ensembles required for reforming, the simple Langmuir form,

$$r = r_0(1-\Theta)^n, \quad [5]$$

was assumed (32), where r_0 is the rate on the clean Ni

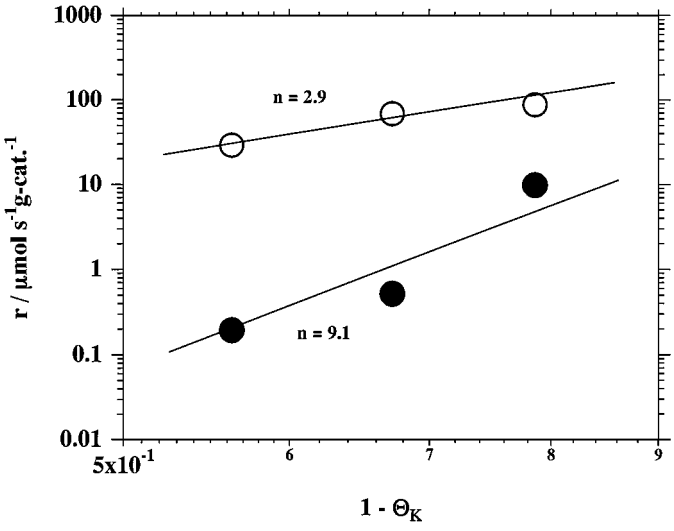

FIG. 14. Influence of potassium on the rates of CO_2 reforming (○) and carbon formation (●) at 773 K.

surface, Θ is the surface coverage of promoter, and n is the number of nickel atoms required for the reaction. Here, the coverage of nickel by potassium, Θ_K, was used. Figure 14 shows ln r vs ln$(1 - \Theta_K)$ plots, from the slope of which the nickel ensemble size n was estimated. The ensemble size was ca. 2.9 for the CO_2-reforming reaction, indicating good agreement with that required for H_2O reforming of methane on sulfur-passivated Ni catalysts ($n = 2.7$) (1). This suggests that the rate-determining step proceeds on ensembles consisting of ca. three nickel atoms. Taking into account that the rate-determining step was suppressed when Θ_K was larger than a threshold value of ca. 0.4 and that a similar ensemble size was obtained when electropositive atoms like K were added to Ni instead of electronegative *S*, it can be considered that the retardation of the rate-determining step above $\Theta_K = 0.4$ is ascribed to physical blockage of the nickel surface by potassium to decrease the concentration of three-atom ensembles. The activation energy was higher on the 10 wt% K-Ni/Al_2O_3 catalyst than on the other catalysts. On 10 wt% K-Ni/Al_2O_3, potassium atoms may also block the Ni ensembles required for C–H bond cleavage in CH_XO_{ads} and, therefore, its dissociation might be retarded. The relationship between the Θ_K and the ensemble size left by potassium addition is not clear at the present stage. To clarify the relationship, theoretical studies using Monte Carlo simulations might be informative (33, 34).

On the other hand, the ensemble size necessary for carbon formation was also estimated from Eq. [5] to be ca. 9.1 (Fig. 14), which is larger than that required for the CO_2-reforming reaction. This suggests that carbon formation proceeds on larger Ni ensembles than CO_2 reforming, as concluded from an analysis of H_2O reforming of CH_4 on *S*-promoted Ni/Al_2O_3 catalysts, on which a power of 6.3 is obtained for carbon formation (1). Although the ensemble size estimated is different in the two sets of studies, it can be considered that large Ni ensembles are necessary for the nucleation of carbon, whereas the CO_2 reforming of CH_4 can proceed on smaller ensembles left after potassium addition. Taking into account that the surface concentration of atomic oxygen formed by the dissociation of CO_2 was not increased by potassium (Table 2), the retardation of carbon accumulation (Fig. 6) cannot be ascribed to the enhancement of the oxidation of $CH_{X,ads}$ by O_{ads} (k_4) but rather must be due to the physical blockage of the nickel surface by potassium; i.e., potassium plays a role in dividing nickel surface into smaller ensembles and, therefore, the carbon deposition should be suppressed. For K-promoted Ni/Al_2O_3 catalysts, the apparent Ni ensemble size during catalyst exposure to the CH_4–CO_2 mixture is considered smaller than that during catalyst exposure only to CH_4, because of the strong adsorption of CO_2 onto the nickel surface modified by potassium, as suggested from Fig. 8a. This may also contribute to the suppression of carbon accumulation more markedly in the presence of CO_2 than in the absence of CO_2 (Fig. 7).

The deposited carbon is also converted to CO by gasification with CO_2 and H_2O, i.e., $C + CO_2 \rightarrow 2CO$ (k_6); however, potassium hardly affected the gasification rate as shown in Fig. 12. The absence of an enhancement effect was also suggested by TPH, as shown in Fig. 13, in which the reactivity of deposited carbon was found to be almost the same on all the catalysts. These results strongly indicate that elemental carbon deposits are not key intermediate species in the CO_2-reforming reaction and that the gasification step (k_6) does not contribute significantly to carbon-free reforming of CH_4. The suppression of coking by potassium is, therefore, mainly ascribed to ensemble control, i.e., dividing the nickel surface into smaller ensembles. In summary, the proposed influences of potassium on the rates of individual steps involved in the CO_2-reforming of methane are summarized in Fig. 1.

CONCLUSIONS

The addition of potassium to Ni/Al_2O_3 catalysts resulted in the reduction of not only the coking activity but also the reforming activity. To investigate the role of potassium in carbon-free reforming, the rates of individual steps involved in the CH_4–CO_2 reaction were examined. The adsorption of CO_2 was enhanced by the presence of potassium; however, CO_2 dissociation to CO and O_{ads} was not significantly affected. This suggests that the enhancement of the oxidation of $CH_{X,ads}$ by O_{ads} is not the cause for the suppression of carbon accumulation on K-promoted Ni/Al_2O_3 catalysts. Carbon-free CO_2 reforming was mainly ascribed to ensemble control; i.e., potassium decreases the concentration of the nickel ensembles necessary for carbon

formation. On the other hand, the rate-determining step, $CH_XO_{ads} \rightarrow CO + x/2H_2$, was suppressed above a nickel coverage of Θ_K = ca. 0.4, and the suppression was again ascribed to physical blockage of the nickel surface by potassium to decrease the number of 3-Ni atom ensembles required for this latter reaction, which is considered a principal cause for the decrease in TOF.

REFERENCES

1. Rostrup-Nielsen, J. R., *J. Catal.* **85**, 31 (1984).
2. Dibbern, H. C., Olesen, P., Rostrup-Nielsen, J. R., Tottrup, P. B., and Udengaard, N. R., *Hydrocarbon Process.* **65**, 3 (1986).
3. Udengaard, N. R., Hansen, J.-H. B., and Hanson, D. C., *Oil Gas J.* **90**, 62 (1992).
4. Gadalla, A. M., and Sommer, M. E., *J. Am. Ceram. Soc.* **72**, 683 (1989).
5. Gadalla, A. M., and Sommer, M. E., *Chem. Eng. Sci.* **44**, 2825 (1989).
6. Bhatta, K. S. M., and Bixon, G. M., *Ind. Eng. Chem. Prod. Res. Dev.* **8**, 324 (1969).
7. Rostrup-Nielsen, J. R., *in* "Catalysis, Science and Technology" (J. R. Anderson and M. Boudart, Eds.), Vol. 5, p. 1. Springer-Verlag, Berlin/New York, 1984.
8. Horiuchi, T., Sakuma, K., Fukui, T., Kubo, Y., Osaki., T., and Mori, T., *Appl. Catal. A: Gen.* **144**, 111 (1996).
9. Tokunaga, O., and Ogasawara, S., *React. Kinet. Catal. Lett.* **39**, 69 (1989).
10. Takano, A., Tagawa, T., and Goto, S., *J. Chem. Eng. Jpn.* **27**, 727 (1994).
11. Cant, N. W., Dümpelmann, R., and Maitra, A. M., *Stud. Surf. Sci. Catal.* **107**, 491 (1997).
12. Balandin, A. A., *in* "Advances in Catalysis" (D. D. Eley, W. G. Frankenburg, V. I. Komarewsky, and P. B. Weisz, Eds.), Vol. 10, p. 96. Academic Press, Orlando, FL, 1958.
13. Kobozev, N. I., *Acta Physicochim.* **9**, 805 (1938).
14. Dowden, D. A., *J. Chem. Soc. London* 242 (1950).
15. Simon, D., and Bigot, E., *Surf. Sci.* **306**, 459 (1994).
16. Lang, N. D., Holloway, S., and Nørskov, J. K., *Surf. Sci.* **236**, 403 (1987).
17. Bengaard, H. S., Alstrup, Ib, Chorkendorff, Ib, Ullmann, S., Rostrup-Nielsen, J. R., and Nørskov, J. K., *J. Catal.* **187**, 238 (1999).
18. Ceyer, S. T., Yang, Q. Y., Lee, M. B., Beckerle, J. D., and Johnson, A. D., *Stud. Surf. Sci. Catal.* **36**, 51 (1987).
19. Rostrup-Nielsen, J. R., *J. Catal.* **31**, 173 (1973).
20. Rostrup-Nielsen, J. R., *J. Catal.* **33**, 184 (1974).
21. Rostrup-Nielsen, J. R., and Christiansen, L. J., *Appl. Catal. A: Gen.* **126**, 381 (1995).
22. Rostrup-Nielsen, J. R., Bak Hansen, J.-H., and Aparicio, L. M., *J. Jpn. Petrol. Inst.* **40**, 366 (1997).
23. Osaki, T., Masuda, H., and Mori, T., *Catal. Lett.* **29**, 33 (1994).
24. Osaki, T., Horiuchi, T., Suzuki, K., and Mori, T., *J. Chem. Soc., Faraday Trans.* **92**, 1627 (1996).
25. Osaki, T., *J. Chem. Soc., Faraday Trans.* **93**, 643 (1997).
26. Osaki, T., Horiuchi, T., Suzuki, K., and Mori, T., *Catal. Lett.* **44**, 19 (1997).
27. Osaki, T., Fukaya, H., Horiuchi, T., Suzuki, K., and Mori, T., *J. Catal.* **180**, 106 (1998).
28. Bradford, M. C. J., and Vannice, M. A., *Appl. Catal. A: Gen.* **142**, 97 (1996).
29. Osaki, T., Horiuchi, T., Sugiyama, T., Suzuki, K., and Mori, T., *Catal. Lett.* **52**, 171 (1998).
30. Horiuchi, T., Hidaka, H., Fukui, T., Kubo, Y., Horio, M., Suzuki, K., and Mori, T., *Appl. Catal. A: Gen.* **167**, 195 (1998).
31. Rostrup-Nielsen, J. R., and Bak Hansen, J.-H., *J. Catal.* **144**, 38 (1993).
32. Maxted, E. B., *Adv. Catal.* **3**, 129 (1951).
33. Anderson, N. T., Topsøe, F., Alstrup, I., and Rostrup-Nielsen, J. R., *J. Catal.* **104**, 454 (1987).
34. Alstrup, I., and Anderson, N. T., *J. Catal.* **104**, 466 (1987).